Hindawi
Journal of Chemistry
Volume 2023, Article ID 5447693, 15 pages
https://doi.org/10.1155/2023/5447693

Research Article

Simple One-Step Synthesis of Nipa Frond-Derived Magnetic Porous Carbon for Decolorization of Acid Yellow 23

Linh Thi Kim Nguyen,[1,2] Long Quang Nguyen,[1,2] Hung Minh Nguyen,[1,2] Thuan Minh Nguyen,[1,2] Hung Hoa Lam,[1,2] Tuyet-Mai Tran-Thuy,[1,2] and Dung Van Nguyen [1,2]

[1]*Faculty of Chemical Engineering, Ho Chi Minh City University of Technology (HCMUT), 268 Ly Thuong Kiet Street, District 10, Ho Chi Minh City, Vietnam*
[2]*Vietnam National University Ho Chi Minh City, Linh Trung Ward, Thu Duc City, Ho Chi Minh City, Vietnam*

Correspondence should be addressed to Dung Van Nguyen; nvdung@hcmut.edu.vn

Received 11 November 2022; Revised 1 February 2023; Accepted 22 March 2023; Published 15 April 2023

Academic Editor: Balasubramani Ravindran

Nipa is an abundant, underutilized palm whose major part is its fronds. Nipa fronds (NF) were, therefore, valorized as a renewable carbon resource for the preparation of advanced magnetic porous carbon (MPC) via simple one-step pyrolysis with $FeCl_3$ addition as a magnetic precursor. Properties of the obtained material were determined by X-ray diffraction (XRD), nitrogen adsorption and desorption isotherms, vibrating sample magnetometer (VSM), scanning electron microscopy (SEM) images, energy-dispersive X-ray (EDX) spectroscopy, and Fourier-transform infrared (FTIR) spectroscopy. XRD results showed that Fe_3O_4 along with Fe^0 particles were formed in the porous carbon base. $FeCl_3$-activation of NF yielded MPC with a high specific surface area (S_{BET}) of 330 m^2/g, a large total pore volume (V_{total}) of 0.26 cm^3/g, and a strong specific saturation magnetization of 7.65 emu/g. Subsequently, MPC was explored for the removal of acid yellow 23 (AY23) using H_2O_2 as an oxidation agent. Before H_2O_2 addition, MPC (0.80 g/L) at pH 3.0 partly eliminated AY23 (initial 100 ppm) with an adsorption capacity of 14.5 mg/g. In further catalytic oxidation with 200 ppm of H_2O_2, MPC removed 89.1% of AY23 within 120 min. Moreover, AY23 decolorization with different MPC samples obeyed pseudo-first-order kinetics, with the greatest rate constant being 0.0186 min^{-1}. Interestingly, the utilized MPC samples could be easily removed from the treated media using a magnet. Altogether, the findings suggest that low-cost magnetic porous carbon produced from one-step pyrolysis of $FeCl_3$-loaded nipa frond might be applied to the treatment of acid yellow 23 in wastewater due to its relative adsorption capacity, efficient catalytic performance, and powerful magnetic separability.

1. Introduction

Today, water pollution is regarded as one of the most significant global challenges, endangering the environment and threatening the lives of millions of people worldwide [1, 2]. During ordinary human activities and industrial operations, a vast range of organic pollutants are released into the water environment [3–5]. Azo dyes are among the most widespread varieties of water pollutants that are discharged through the effluents of different industrial processes [6, 7]. Because the bulk of the dyes have stable and complex molecular structures, it becomes challenging to degrade them using conventional chemical and biological processes [8]. Many of these substances are poisonous, carcinogenic to living organisms, and detrimental to aquatic life [9]. Acid yellow 23 (AY23) is also known as tartrazine, which is a sulfonated azo dye widely utilized in the cosmetics, pharmaceutical, and food industries [3, 10]. Because of its high solubility in water, AY23 is more likely to be found as a pollutant in industrial wastewater. AY23 is toxic at high concentrations and appears to be hazardous to human health, potentially causing hyperactivity, migraine, asthma, urticaria, angioedema, thyroid cancer, etc. [1, 11]. In light of these possible risks, it is essential to find an effective and

sustainable solution to treat AY23 in wastewater before discharging it into the environment.

Because AY23 is recalcitrant to biodegradation, adsorption and advanced oxidation are common technologies for its treatment [1, 8, 11–13]. Adsorption is generally simple, but it is unable to mineralize organic molecules. As a result, additional treatment of the used adsorbents may be required. In contrast, advanced oxidation processes (AOPs) have proven their ability to decompose and mineralize diverse organic contaminants. Among AOPs, the low-cost Fenton process, which uses Fe^{2+} ions as a catalyst and H_2O_2 as an oxidation agent, has been widely utilized [14]. In this catalysis, Fe^{2+} ions can accelerate the breakdown of H_2O_2 into powerful hydroxyl radicals (·OH) for nonselective oxidation of organic species [15]. However, Fe^{2+} ions can generate waste sludge that is difficult to reuse [16]. In order to overcome the aforementioned issues of homogeneous Fenton oxidation, considerable research has been conducted on the heterogeneous Fenton-like processes utilizing Fe-based solid catalysts such as Fe_2O_3, Fe_3O_4, FeOOH, and zero-valent Fe^0 [17]. These Fe-based particles are affordable, stable, easily prepared, and magnetically separable [18, 19]. Nevertheless, the particles may aggregate during use, reducing their catalytic activity [20, 21]. Hence, they must be dispersed onto appropriate supports. Due to their favorable interaction with organic molecules in wastewater, carbon-based materials have been extensively explored as effective supports for Fe-based particles [22]. Compared with synthetic carbon materials like graphene, carbon nanotubes, and nanoporous carbon, biomass-derived porous carbon (PC) is recognized as an inexpensive, sustainable, and eco-friendly support for heterogeneous Fenton catalysts [15, 23, 24].

Biomass-derived PC materials (biochar and activated carbon) are prepared from the carbonization of various biomass resources [25, 26]. Owing to their advantageous physicochemical characteristics, porous structure, and multiple functional groups [27, 28], PCs are utilized for a variety of applications, such as wastewater treatment, gas storage and separation, soil remediation, and catalytic supports [22, 29]. However, separating and recovering PCs is challenging. Conventional separation techniques are either expensive or ineffective, severely limiting their use [22]. Recent studies suggest dispersing magnetic particles such as Fe_3O_4, Fe_2O_3, and Fe^0 on PC to generate magnetic porous carbon (MPC) [30, 31]. In this manner, magnetic particles can facilitate the separation and recovery of MPC through external magnetic fields [32, 33]. On the other hand, the carbon support can fix magnetic particles and prevent their aggregation into bigger particles [20, 34]. Overall, the advanced MPC combines desirable physicochemical properties, including the porous structure and functional groups of carbon supports, as well as the magnetic separability and catalytic activity of Fe-based particles [35–37].

MPC is traditionally prepared in two steps: pyrolysis of biomass into pristine PC and chemical dispersion of magnetic particles over pristine PC [31]. In general, these procedures are time- and energy-consuming [15]. Additionally, magnetic particles could obstruct existing pores in carbon supports, thereby reducing their surface area and pore volume. Recently, an advanced route has been developed for the one-pot synthesis of MPC via direct $FeCl_3$-activation of biomass [35, 38]. First, magnetic precursors are impregnated into biomass feedstocks. Subsequently, the resulting mixtures are pyrolyzed into MPC [20, 39, 40]. The advanced procedure could not only load magnetic particles but also activate carbon surfaces simultaneously during pyrolysis. According to Bedia et al. [41], $FeCl_3$-activation of biomass yields MPC with well-developed porosity and well-dispersed iron-based particles. Do et al. [36] proved that MPC prepared via one-step pyrolysis showed high catalytic activity, long reusability, and good stability in the Fenton-like treatment of Orange G. In spite of this, there are still few reports on MPC fabricated through $FeCl_3$-activation of biomass resources for use in catalysis. Further research on AY23 treatment to explore MPC catalysts is necessary.

It is found that $FeCl_3$-activation of various biomass resources can yield MPCs with a diversity of porous structures, functional groups, and iron-based products which significantly affect their magnetic properties, adsorption capacities, and catalytic activities [22, 36, 42]. To expand the selection of MPC for further applications, increased research on the fabrication conditions, properties, and catalytic performance of MPC from newly prospective biomass resources is desired. Nipa (*Nypa fruticans*) is a monoecious palm that flourishes in soft mud and slow-moving tidal regions, including river estuaries, coasts, and mangrove forests [43, 44]. The palm can be found in a variety of tropical locations, like Nigeria, Sri Lanka, India, Bangladesh, Myanmar, Thailand, Cambodia, Malaysia, Indonesia, Papua New Guinea, Australia, the Philippines, and Vietnam [45–47]. Unlike most palms, nipa is trunkless. It consists of only fronds, leaves, and flower stalks above the ground [48, 49]. Nowadays, nipa is considered an unexploited species. Most biomass parts of nipa are left to decay in their living environment, with limited use [48, 50]. Nipa fronds (NFs), the main part of the palm, can therefore be an abundant and available raw material for further use. In this study, NF was valorized for the first time as a newly renewable carbon source for the one-step synthesis of MPC. The properties of the as-synthesized MPC were thoroughly investigated and discussed.

2. Materials and Methods

2.1. Materials. Nipa fronds were gathered from Chau Thanh District, Dong Thap Province, Vietnam. The raw material was first rinsed with tap water and distilled water. It was then dried in an oven at 105°C for 24 h. Next, NF was sliced, ground, and sieved to a size of 0.25–0.50 mm before being sealed in a plastic bag for further usage. $FeCl_3.6H_2O$ (≥99.0%), NaOH (≥96.0%), HCl (36.0–38.0%), H_2O_2 (≥30.0%), $Na_2S_2O_3.5H_2O$ (≥99.5%) were purchased from Xilong Scientific, China. Acid yellow 23 (tartrazine) was procured from Roha Dye Chem, India. All chemicals were used as received without any additional purification.

2.2. Preparation of Magnetic Porous Carbon. Initially, 3.00 g of dried nipa frond powder and 0.15, 0.30, or 0.60 g of $FeCl_3$ were added to 70 mL of distilled water. The mixture was stirred at room temperature for 24 h, and then dried at 105°C for 24 h. The sample was put in a glass reaction tube (diameter: 3 cm × length: 25 cm) with a continuous nitrogen flow (50 mL/min). The mixture was heated to 600°C at a rate of 10°C/min and kept at that temperature for 0.5, 1.0, 2.0, or 4.0 h. After pyrolysis, the reaction tube was cooled to ambient temperature. Pyrolysis efficiency was evaluated by the mass ratio of the obtained nonwashed MPC and the $FeCl_3$-loaded NF (equation (1)). MPC was thereafter rinsed with distilled water many times until the pH became neutral. A nonwashed sample was also prepared to clarify the impact of residual $FeCl_3$ on catalytic activity. As-prepared MPC samples are denoted as MPC-Rx-yh, where x is the $FeCl_3$/NF mass ratio and y is the pyrolysis time (h). In order to compare the catalytic activities, porous carbon (abbreviated as PC) was prepared by directly pyrolyzing NF under the same condition but without adding $FeCl_3$.

$$\text{Pyrolysis efficiency } (\%) = \frac{\text{Non} - \text{washed MPC (g)}}{\text{FeCl}_3 - \text{loaded NF (g)}} \times 100\%. \tag{1}$$

2.3. Characterization of Magnetic Porous Carbon. X-ray diffraction (XRD) of MPC samples was performed using a Bruker AXS D8 diffractometer with Cu Kα radiation ($\lambda = 1.5418$ Å) at a scan rate of 1°/min over a 2θ range of 10–75°. Nitrogen adsorption and desorption isotherms of PC and MPC were performed at 77 K on a Micromeritics Gemini VII 2390T instrument. The samples were outgassed at 250°C for 3 h. Pore size distribution was determined by BJH method. Specific surface area (S_{BET}) was calculated by Brunauer–Emmett–Teller equation. Total pore volume (V_{total}) was measured at $P/P_o = 0.995$. Micropore volume (V_{micro}) and external surface area (S_{ext}) were determined by t-plot method. Meso-macropore volume ($V_{meso\text{-}macro}$) was calculated from the difference between V_{total} and V_{micro}. Micropore surface area (S_{micro}) was obtained by subtracting S_{ext} from S_{BET}. The average pore size (d_{pore}) was calculated from $4V_{total}/S_{BET}$. The scanning electron microscope (SEM) images were observed with a FE-SEM S-4800. An energy-dispersive X-ray (EDX) spectroscopy instrument (JSM-IT200) was used to examine the elemental mapping of MPC. Functional groups on MPC surface were characterized by Fourier-transform infrared (FTIR) spectroscopy using a spectrometer (VERTEX 70, Bruker Optics). Magnetic properties of MPC were determined by a vibrating sample magnetometer (VSM) at room temperature. Iron content in MPC was determined by the original ferrozine method [51].

2.4. Acid Yellow 23 Removal by Magnetic Porous Carbon. Acid yellow 23 decolorization was performed in a 600-mL glass flask at ambient temperature (30°C). 260 mL of AY23 (100 ppm) was prepared in the flask. Then, different MPC dosages were added, and a magnetic stirrer was used to mix the obtained suspension continuously. HCl (0.1 M) and NaOH (0.1 M) solutions were used to adjust the initial pH values of the mixture. After the adsorption step in the first 10 min, different H_2O_2 dosages were rapidly poured into the suspension for the further oxidation step. At different time intervals, each 2.5 mL of sample was withdrawn from the reaction mixture and added to a solution of 1.0 mL of $Na_2S_2O_3$ (0.001 M) and 0.5 mL of NaOH (0.01 M) to remove excess H_2O_2 and adjust pH. A magnet was used to support the separation of the MPC catalyst from the suspension. Finally, AY23 concentrations were measured by a UV-Vis Spectronic Genesys 2 PC at 430 nm. The adsorption capacity and decolorization efficiency of AY23 over MPC were calculated by the following equations:

$$\begin{aligned} \text{adsorption capacity}\left(\frac{\text{mg}}{\text{g}}\right) &= \frac{C_0 - C_{10}}{C_{MPC}}, \\ \text{decolorization efficiency } (\%) &= \frac{C_0 - C_{120}}{C_0} \times 100\%, \end{aligned} \tag{2}$$

where C_{MPC} was MPC dosage (g/L), C_0, C_{10}, and C_{120} (ppm) were AY23 concentrations at the beginning, after 10 min of treatment, and after 120 min of treatment, respectively.

3. Results and Discussion

3.1. Characteristics of Magnetic Porous Carbon

3.1.1. Effect of Washing on XRD Patterns of MPC. As reported in the literature [35, 36, 52], different Fe-based particles could be generated during the pyrolysis of $FeCl_3$-loaded biomass as follows:

$$\text{biomass} \longrightarrow H_2O, CO, C, H_2 \tag{3}$$

$$FeCl_3 + H_2O \longrightarrow FeOCl.H_2O \;\&\; Fe(OH)_3 \longrightarrow FeO(OH) \longrightarrow Fe_2O_3 \tag{4}$$

$$Fe_2O_3 + CO, C, H_2 \longrightarrow Fe_3O_4 + CO, C, H_2 \longrightarrow Fe \tag{5}$$

Equations (3)–(5) indicate that the formation ability of Fe-based products on MPC could depend on the products of carbonization. As a matter of fact, a lack of water vapor could not completely convert the $FeCl_3$ reactant into Fe-based products. Hence, the existence of Fe-based matters in nonwashed and washed MPC-R0.2–2.0 h was explored by XRD (Figure 1). Both samples showed characteristic peaks at 30.40, 35.32, 53.48, 56.96, and 62.44° indexed to the (220), (311), (422), (511), and (440) planes of Fe_3O_4 (JCPDS 19-0629), respectively. Similarly, a small peak at 44.79° from the (110) plane of zero-valent Fe^0 (JCPDS 006-0696) was observed in both samples. Reversely, the washed MPC sample lost obvious characteristic peaks at 31.73 and 45.45°, which could represent (113) and (116) planes of residual $FeCl_3$ (ICDD 00-001-1059) [53–56]. In addition, the brown color of freshly precipitated $Fe(OH)_3$ was observed by adding the nonwashed MPC-R0.2-2.0 h sample to an aqueous NaOH solution (Figure 2(a)). pH measurements of the mixture also revealed an acidic medium caused by Fe^{3+} leaching. To ensure that all residual $FeCl_3$ was removed from MPC, washing was repeated until the solution was colorless with the NaOH test (Figure 2(b)) and neutral with the pH test. In later parts, only washed MPC samples were used.

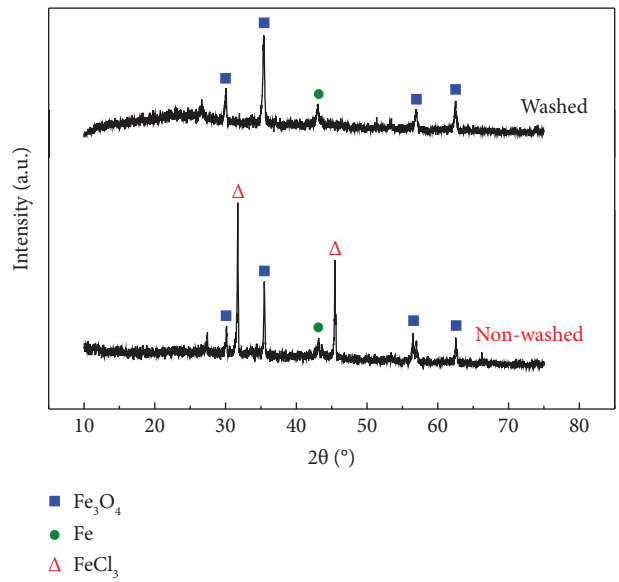

Figure 1: XRD patterns of nonwashed and washed MPC-R0.2-2.0 h samples.

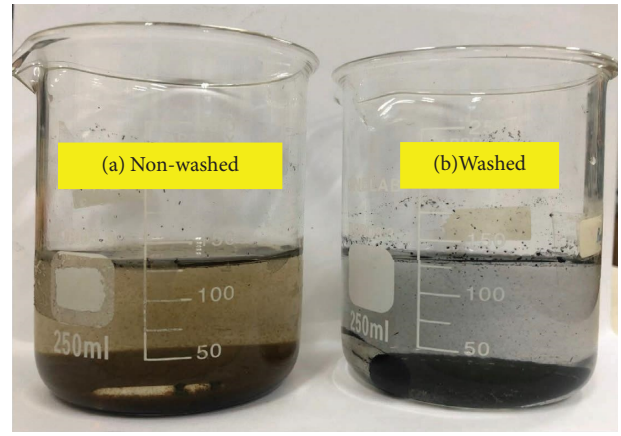

Figure 2: Color change after adding nonwashed and washed MPC-R0.2-2.0 h samples to aqueous NaOH solutions. (a) Nonwashed. (b) Washed.

3.1.2. Effect of Pyrolysis Time on XRD Patterns of MPC. As presented in Figure 3, Fe_3O_4 and Fe^0 crystals were formed in all MPC samples prepared from different pyrolysis time. With high intensity of sharp peaks, Fe_3O_4 could be the major Fe-based product. A minor part of Fe_3O_4 could be further reduced into Fe^0 over carbon base. As the pyrolysis time rose from 0.5 to 2.0 h, the formation of Fe_3O_4 crystals was slightly improved. Reversely, a longer pyrolysis time at 4.0 h did not actually yield better Fe_3O_4 crystals but seemed to enhance Fe^0 crystals. These Fe_3O_4 crystals might also be converted into other materials in crystal or amorphous phases. The biomass carbonization might be complete, and prolonging pyrolysis time might not offer more substances for converting $FeCl_3$ into Fe_3O_4, except for carbon. This finding has been discussed in such reports [20, 57].

Table 1 showed that the pyrolysis efficiency decreased from 62 to 56% as the pyrolysis time was prolonged from 0.5 to 4.0 h. During pyrolysis, the biomass carbonization, the decomposition of $FeCl_3$, and the activation of porous carbon by Fe-based compounds could release volatile matters such as H_2O, CO, CO_2, and HCl (equations (3)–(5)), triggering a decrease in pyrolysis efficiency [20]. Nevertheless, there was a very slight decrease in pyrolysis efficiency between 2.0 h (57%) and 4.0 h (56%). The results proved that the pyrolysis was nearly complete after 2.0 h. Overall, the appropriate pyrolysis time for forming Fe_3O_4 crystals might be around 2.0 h.

3.1.3. Effect of $FeCl_3$/NF Mass Ratio on XRD Patterns of MPC. Figure 4 shows that increasing the $FeCl_3$/NF mass ratio from 0.05 to 0.1 resulted in higher Fe_3O_4 peaks. However, when the $FeCl_3$/NF mass ratio was increased from 0.1 to 0.2, the trend was reversed. According to Do et al. [36], the lack of water released from the biomass carbonization at high ratios may suppress the conversion of $FeCl_3$ to Fe_3O_4. Table 1 reveals that the pyrolysis efficiency improved as the $FeCl_3$/NF mass ratio increased. Higher residual solids indicated that reactions occurring during pyrolysis were weakened [20, 36].

3.1.4. Porous Properties of MPC. Figure 5 presents the nitrogen adsorption-desorption isotherm of MPC-R0.1–2.0 h. It is found to be a narrow hysteresis loop at relative pressure (P/P_o) from 0.40 to 0.995, possibly relating to capillary condensation in slit-shaped pores [58]. Interestingly, BJH analysis revealed that MPC has a hierarchically micro-meso-macro porous structure. Meso-macropores contribute 0.13 cm^3/g, which corresponds to 50% of V_{total} (Table 2). As compared to PC, MPC has a much higher V_{micro} but a similar $V_{meso\text{-}macro}$. As a result, the S_{BET} and V_{total} of MPC are 330 m^2/g and 0.26 cm^3/g, which are 2.2- and 1.4-fold higher than those of PC, respectively. These results indicate

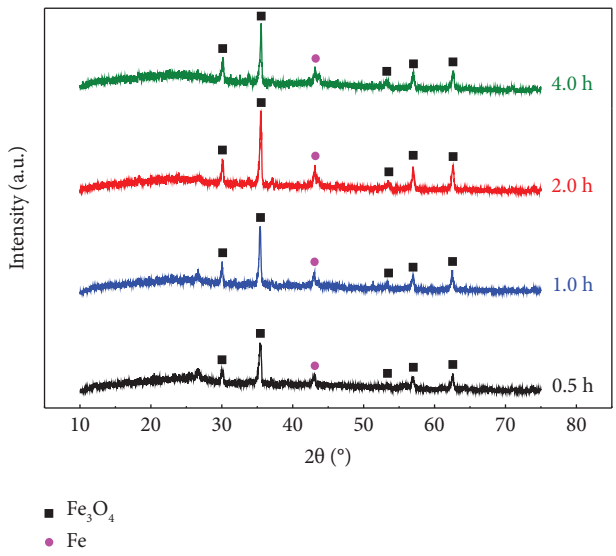

FIGURE 3: XRD patterns of MPC-R0.2-yh samples prepared from different pyrolysis time (y).

that the presence of Fe-based compounds could mainly activate micropores during biomass carbonization [35, 36, 59, 60]. Moreover, the one-step strategy increased S_{BET} and V_{total} of MPC, as reviewed before.

3.1.5. FTIR Spectroscopy of MPC. Functional groups on MPC-R0.1–2.0 h surface were qualitatively analyzed by FTIR spectroscopy (Figure 6). Different adsorption peaks were recorded, including 3431 cm^{-1} (O-H stretching vibrations), 2890 cm^{-1} (C-H stretching vibrations), 2351 cm^{-1} (O=C=O stretching vibrations), 1630 cm^{-1} (O-H bending vibrations), 1537 cm^{-1} (C=C stretching vibrations in aromatic rings), 1136 cm^{-1} (C-O stretching vibrations), and 888 cm^{-1} (C-H bending vibrations of aromatics) [33, 35, 36, 61–63]. Stretching vibrations of aliphatic C-H at 2890 cm^{-1} were very weak, and stretching vibrations of C=O at around 1700 cm^{-1} were lost, demonstrating that the carbonization of NF was nearly complete [52]. Interestingly, the presence of polar oxygen-containing functions on the MPC surface might enhance its interactions with aqueous organic pollutants [36, 64].

3.1.6. SEM Images of MPC. SEM images at different magnifications were used to observe the surface morphology of MPC-R0.1–2.0 h (Figure 7). The material has a smooth surface with flaky fragments. Notably, it seems hard to find aggregated Fe_3O_4 and Fe^0 particles on the surface of MPC. Instead of adhering to the carbon surface, Fe-based particles formed by direct pyrolysis of $FeCl_3$-loaded biomass can be encapsulated within the carbon base, as stated in such reports [36, 41]. Consequently, the particles are able to sustain a steady performance over an extended period of time.

3.1.7. EDX Spectroscopy and Elemental Mapping of MPC. Figure 8 depicts the EDX spectroscopy and elemental mapping of MPC-R0.1–2.0 h. C, Fe, and O are the most abundant elements on the MPC surface, accounting for 76.65, 6.63, and 11.37 wt%, respectively. This surface Fe content was slightly lower than the bulk Fe content (8.7 wt%) determined by the original ferrozine method. This result suggests that the Fe element may be embedded within the carbon structure. Furthermore, the atom ratio of O/Fe on the surface of MPC was 6.0, which was significantly more than that of Fe_3O_4. Hence, oxygen could exist in both Fe_3O_4 and oxygen functional groups.

According to Tamunaidu and Saka [48], Na, K, Mg, Ca, P, S, Cl, and Si elements were detected in nipa fronds from the Philippines. Similar inorganic elements were found in NF from Thailand [49]. In this research, except for Na and K, the remaining elements were detected in NF-derived MPC. Na and K may have been removed by washing or were not present in NF feedstock. Nevertheless, Cl might partially or completely originate from the added $FeCl_3$. As previously stated, MPC was cleaned until no further Fe^{3+} and Cl^- leaching occurred. Thus, these inorganic elements might be firmly immobilized in the inner parts of the carbon structure by strong mechanical or chemical bonds [20]. Lastly, element mapping showed that Fe sites as well as other available elements (O, Mg, Ca, Cl, Si, P, and S) were well dispersed on the MPC surface (C). The uniform Fe distribution may be due to the efficiency with which $FeCl_3$ was preloaded into NF prior to pyrolysis.

3.1.8. Magnetic Properties of MPC. As shown in Figure 9, MPC could be effectively attracted by a magnet. It contributes significantly to the separation and recovery of MPC from certain suspensions. As previously described, MPC was separated from the treated sample using a magnet prior to the analyzing step. Moreover, the magnetic hysteresis curve revealed that MPC was superparamagnetic due to its magnetizability and demagnetizability. These magnetic properties could result from both Fe_3O_4 and Fe^0 particles coexisting in MPC [65, 66]. With only 8.7 wt% Fe, the specific saturation magnetization (M_S) reached 7.65 emu/g (Table 2), not much different from other reports for MPC [31, 35]. Assuming that all Fe in MPC is either 100% Fe_3O_4 or 100% Fe^0, their corresponding saturation magnetizations would be 88 or 64 emu/g, respectively. These values are roughly comparable to those of Fe_3O_4 [67–69] and Fe^0 nanoparticles [70–72].

3.2. Removal of Acid Yellow 23 by MPC Catalyst

3.2.1. Effect of Washing MPC Catalyst. The decolorization of acid yellow 23 catalyzed by nonwashed and washed MPC samples was compared in Figure 10. In both of these experiments, the pH value of the AY23 solution was adjusted to 6.0 before adding the MPC samples. For washed MPC, AY23 decolorization occurred slowly during treatment. The high pH of the suspension was maintained, and almost no Fe^{3+} leaching was detected by adding NaOH solution at the end of the oxidation step. In contrast, nonwashed MPC accelerated AY23 decolorization significantly. Fe^{3+} leaching resulted in homogeneous mechanisms and low pH, both of

Table 1: Pyrolysis efficiency of $FeCl_3$-loaded nipa frond.

Samples	Pyrolysis time (h)	$FeCl_3$/NF (w/w)	Pyrolysis efficiency (%)
MPC-R0.2–0.5 h	0.5	0.2	62
MPC-R0.2–1.0 h	1.0		60
MPC-R0.2–2.0 h	2.0		57
MPC-R0.2–4.0 h	4.0		56
MPC-R0.05–2.0 h	2.0	0.05	46
MPC-R0.1–2.0 h		0.1	53
MPC-R0.2–2.0 h		0.2	57

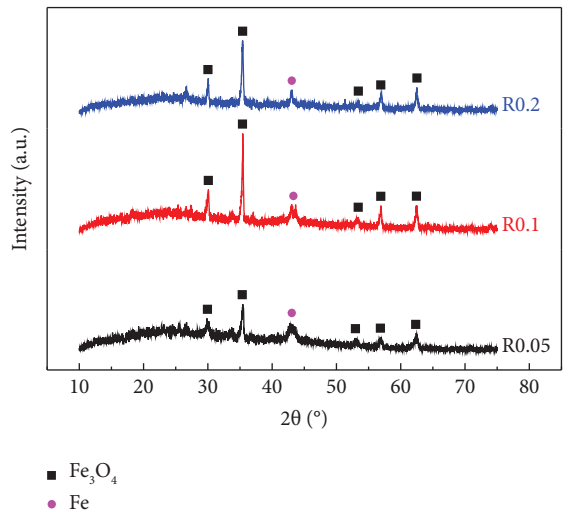

Figure 4: XRD patterns of MPC-Rx-2.0 h samples prepared from different $FeCl_3$/NF mass ratios (x).

which were favorable for Fenton-like reactions. This could lead to the misconception that MPC exhibits effective catalytic activity throughout a broad pH range. To assess right catalytic activity as well as achieve stable heterogeneous catalysis, all MPC samples were meticulously washed to remove all remaining $FeCl_3$.

3.2.2. Effect of MPC Prepared from Different Pyrolysis Time. Figure 11 presents the influence of MPC samples obtained at different pyrolysis time on the adsorption capacity and catalytic decolorization of AY23. In the first adsorption step, the adsorption processes occurred rapidly and nearly achieved equilibrium in 10 min. As the pyrolysis time increased from 0.5 to 4.0 h, the adsorption capacity gradually rose from 5.6 to 11.3 mg/g (Table 3). Pyrolysis time could affect the porous structure of MPC [35], potentially resulting in AY23 adsorption. Regarding the adsorption mechanisms, AY23 might interact with the MPC surface via hydrogen bonding, π-π stacking interaction, and electrostatic interaction [35, 73]. Contrarily, ionic Fe_3O_4 and metallic Fe^0 crystals might not bind organic AY23 molecules as well. This demonstrated that, under proper conditions, MPC could be a practical adsorbent for AY23 remediation. However, the advantage of MPC comes from its catalytic activity for AY23 decolorization.

Fe_3O_4 and/or Fe^0 particles residing in MPC might accelerate the breakdown of H_2O_2 into ·OH, according to the following equations [36, 74]:

$$\begin{aligned}
&Fe(0) + H_2O_2 + 2H^+ \longrightarrow Fe(II) + 2H_2O\\
&Fe(II) + H_2O_2 \longrightarrow Fe(III) + {\cdot}OH + OH^-\\
&Fe(III) + H_2O_2 \longrightarrow Fe(II) + H^+ + {\cdot}OOH\\
&\text{Organic pollutants} + {\cdot}OH \longrightarrow \text{Intermediates} \longrightarrow CO_2 + H_2O
\end{aligned} \tag{6}$$

As described in XRD results, Fe_3O_4 and Fe^0 crystals, which could be the dominant catalytic sites of MPC, were grown during the pyrolysis. The growth was practically complete after 2.0 h and did not improve much thereafter. As a result, when the pyrolysis time was prolonged from 0.5 to 2.0 h, the catalytic activity of the MPC samples increased significantly, leading to an increase in the decolorization efficiency of AY23 from 33.2 to 81.9% (Table 3). However, the decolorization rate catalyzed by MPC-R0.1–4.0 h was not much higher than that catalyzed by MPC-R0.1–2.0 h. To save energy for the synthesis of MPC, the appropriate pyrolysis time was 2.0 h.

3.2.3. Effect of MPC Prepared from Different $FeCl_3$/NF Mass Ratios. AY23 decolorization was explored with MPC catalysts prepared from different $FeCl_3$/NF mass ratios of 0.05, 0.1, and 0.2 (Figure 12). To assess the role of Fe-based catalyst and porous carbon support, a porous carbon sample without Fe (PC-2.0 h) was used as a reference. In the absence of Fe, PC eliminated a negligible amount of AY23 through adsorption rather than catalytic oxidation. In contrast, all MPC samples exhibited robust AY23 decolorization. These results suggest that the catalytic activities of MPC are solely derived from Fe sites in Fe_3O_4 and Fe^0 particles. However, the porous system and functional groups

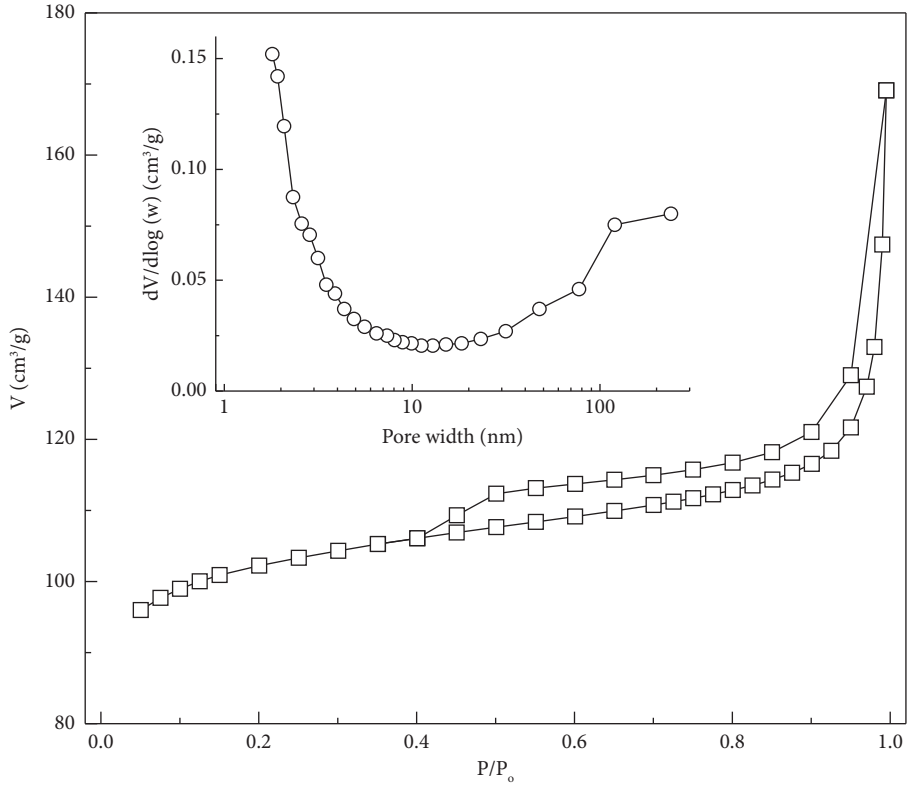

Figure 5: Nitrogen adsorption-desorption isotherm and BJH pore size distribution of MPC-R0.1–2.0 h.

Table 2: Properties of PC-2.0 h and MPC-R0.1–2.0 h.

Samples	Fe content (wt%)	S_{BET} (m^2/g)	S_{micro} (m^2/g)	S_{ext} (m^2/g)	V_{total} (cm^3/g)	V_{micro} (cm^3/g)	$V_{meso\text{-}macro}$ (cm^3/g)	d_{pore} (nm)	M_S (emu/g)
PC-2.0 h	n.a.	151	67	84	0.18	0.03	0.15	4.8	n.a.
MPC-R0.1–2.0 h	8.7	330	264	66	0.26	0.13	0.13	3.2	7.65

N.A.: not analyzed.

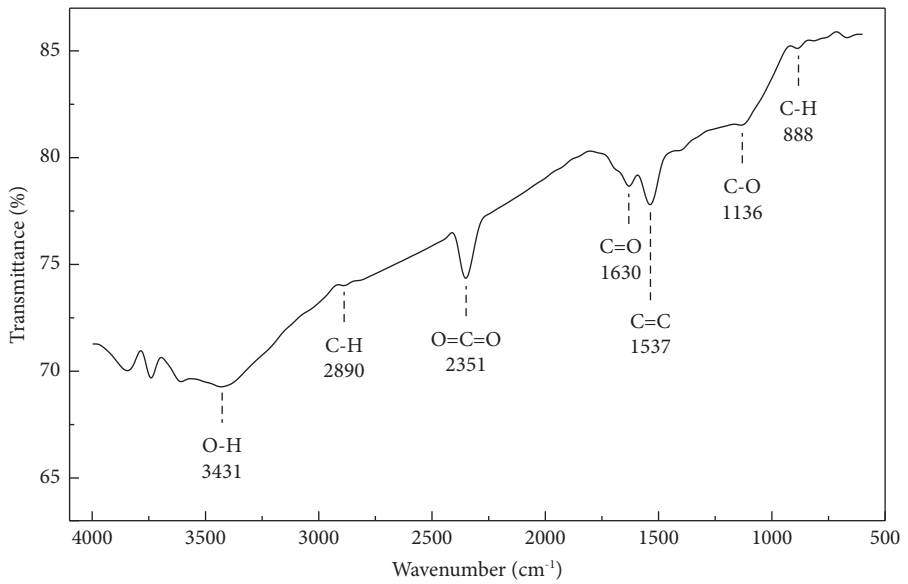

Figure 6: FTIR spectroscopy of MPC-R0.1–2.0 h.

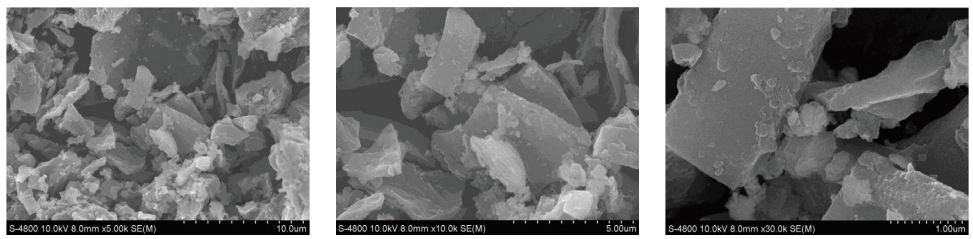

(a) (b) (c)

Figure 7: SEM images of MPC-R0.1–2.0 h at different magnifications (×5,000, ×10,000, and ×30,000).

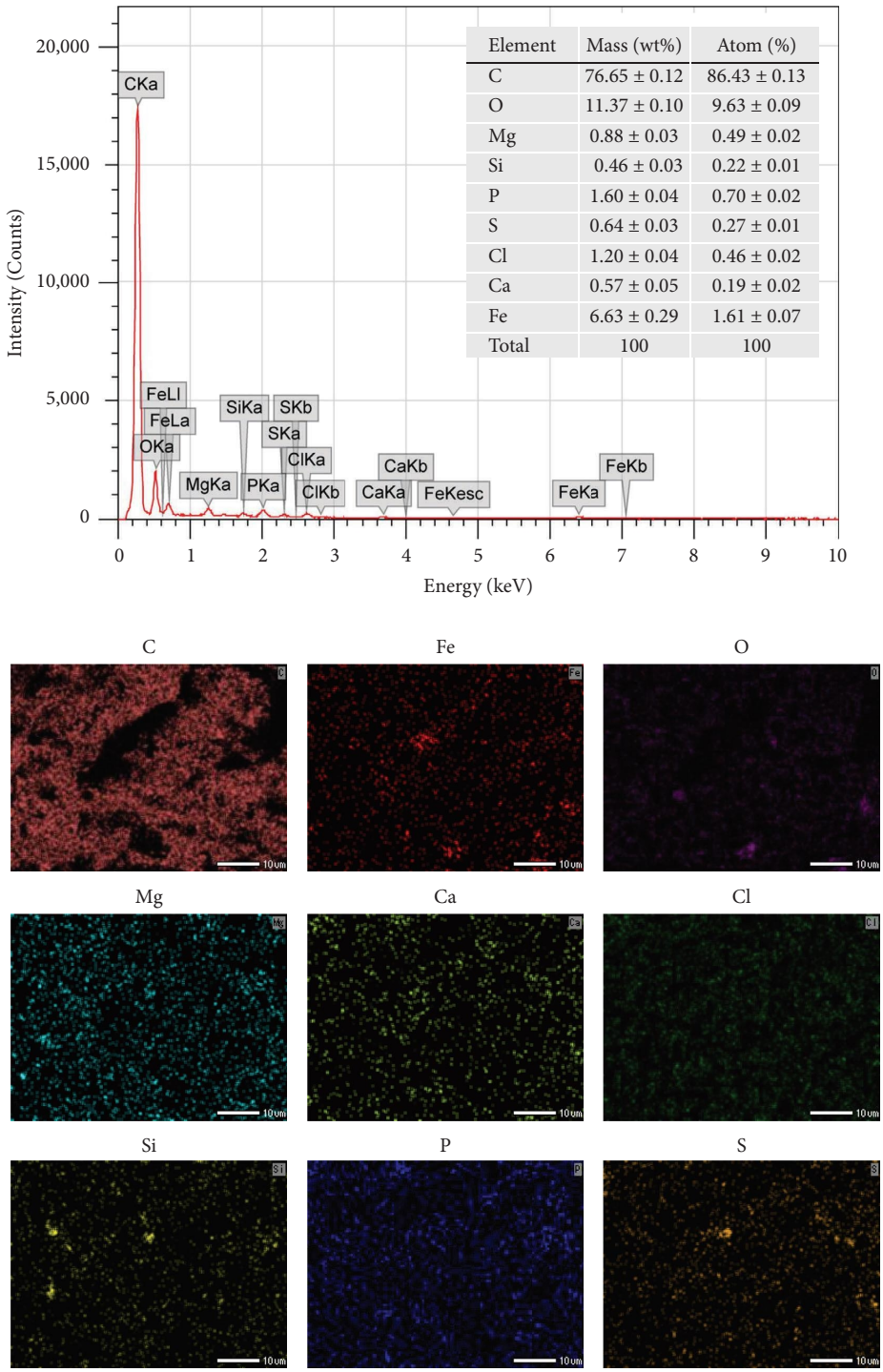

Figure 8: EDX spectroscopy and elemental mapping of MPC-R0.1–2.0 h.

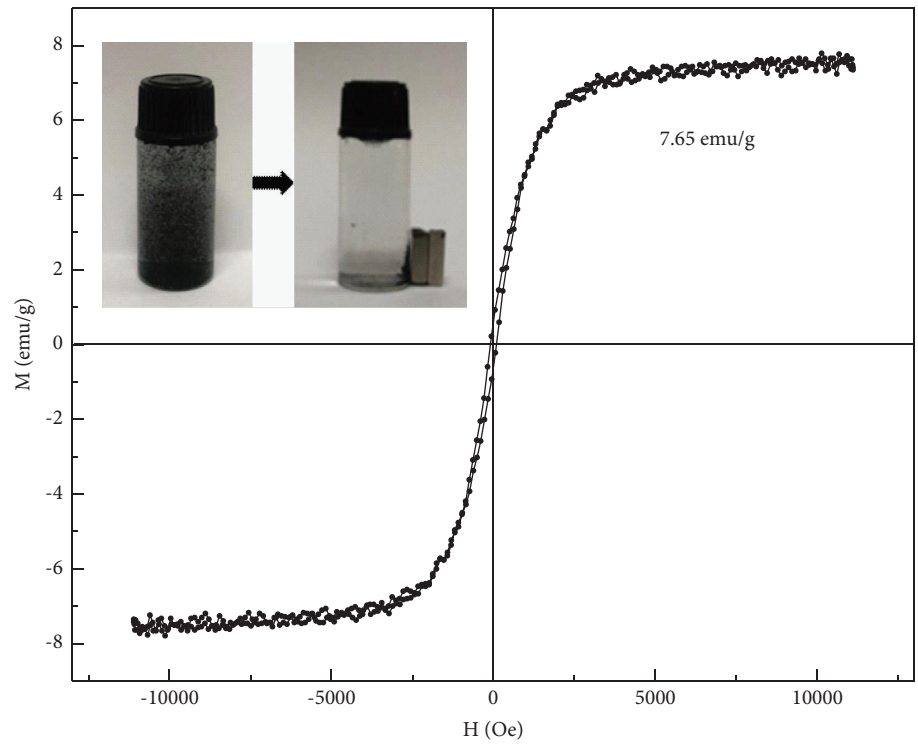

Figure 9: Magnetic hysteresis loop of MPC-R0.1–2.0 h.

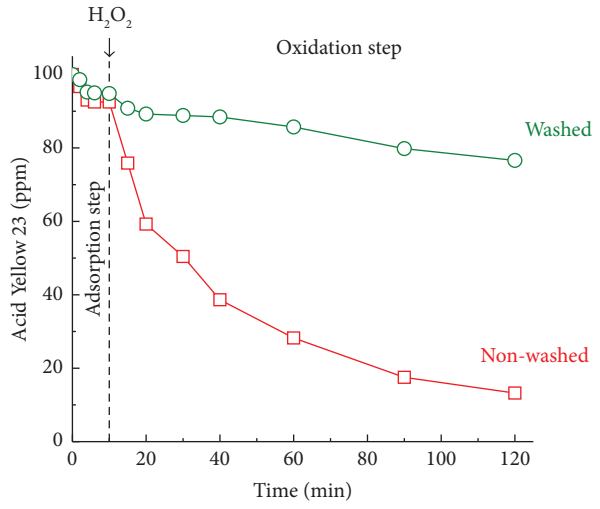

Figure 10: Effect of washing MPC catalyst on AY23 decolorization (0.80 g/L MPC-R0.2–2.0 h, initial pH 6.0, 200 ppm H_2O_2).

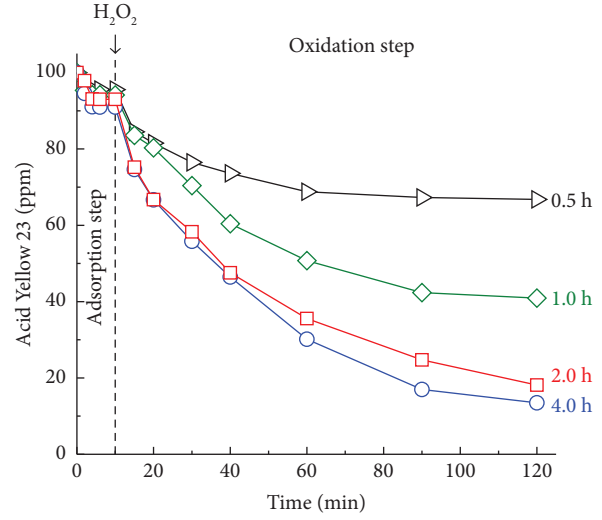

Figure 11: Effect of MPC catalysts prepared from different pyrolysis time on AY23 decolorization (0.80 g/L MPC-R0.2-yh, pH 3.0, 200 ppm H_2O_2).

of the carbon support might play a certain role in the catalysis process, such as facilitating species in mass transfer and surface interaction [36]. When the $FeCl_3$/NF mass ratio increased from 0.05 to 0.2, the catalytic activity of the obtained MPC samples did not differ significantly. A higher $FeCl_3$/NF mass ratio could result in more Fe catalytic sites in MPC, leading to greater AY23 decolorization. Notwithstanding, ·OH radicals might be diminished by excessive Fe, as expressed in the following reaction [75, 76]:

$$\mathrm{Fe(II)} + \cdot\mathrm{OH} \longrightarrow \mathrm{Fe(III)} + \cdot\mathrm{OH}^{-}. \quad (7)$$

3.2.4. Effect of MPC Dosage. The effect of MPC dosage on AY23 decolorization is shown in Figure 13 and Table 3. Without any MPC catalyst, H_2O_2 was incapable of degrading AY23. Conversely, AY23 was swiftly decolorized when MPC was added. These results revealed that the presence of MPC catalyst played a crucial role in decolorizing AY23, as discussed previously. As expected, the decolorization rate increased when the MPC dosage was changed from 0.40 to 1.20 g/L. After 120 min, the decolorization efficiencies of 0.40 g/L, 0.80 g/L, and 1.20 g/L MPC were 64.7, 89.1, and

Table 3: Adsorption capacity and catalytic activity of PC and MPC samples on acid yellow 23.

Samples	MPC (g/L)	pH	H_2O_2 (ppm)	Adsorption (after 10 min)		Oxidation (after 110 min)		Decolorization efficiency (%)
				AY23 (ppm)	Adsorption capacity (mg/g)	AY23 (ppm)	AY23 removal (%)	
MPC-R0.2–0.5 h	0.8	3.0	200	95.6	5.6	66.8	28.8	33.2
MPC-R0.2-1.0 h				94.1	7.3	40.9	53.2	59.1
MPC-R0.2–2.0 h				93.0	8.7	18.1	74.9	81.9
MPC-R0.2–4.0 h				91.0	11.3	13.5	77.5	86.5
PC-2.0 h	0.8	3.0	200	92.3	9.6	88.2	4.1	11.8
MPC-R0.05–2.0 h				89.5	13.2	19.9	69.6	80.1
MPC-R0.1–2.0 h				88.4	14.5	10.9	77.5	89.1
MPC-R0.2–2.0 h				93.0	8.7	18.1	74.9	81.9
MPC-R0.1–2.0 h	0.00	3.0	200	100.0	0.0	94.4	5.6	5.6
	0.40			90.7	11.6	35.3	55.4	64.7
	0.80			88.4	14.5	10.9	77.5	89.1
	1.20			85.3	18.4	8.8	76.5	91.2
MPC-R0.1–2.0 h	0.80	2.0	200	85.5	18.1	5.5	80.1	94.5
		3.0		88.4	14.5	10.9	77.5	89.1
		3.5		93.4	8.2	62.2	31.2	37.8
		4.0		95.1	6.1	75.6	19.5	24.4
		6.0		94.8	6.5	76.6	18.2	23.4
		10.0		95.1	6.1	83.5	11.6	16.5
MPC-R0.1–2.0 h	0.80	3.0	100	88.3	14.7	45.8	42.4	54.2
			150	88.9	13.8	29.5	59.4	70.5
			200	88.4	14.5	10.9	77.5	89.1
			300	88.4	14.5	19.9	68.5	80.1

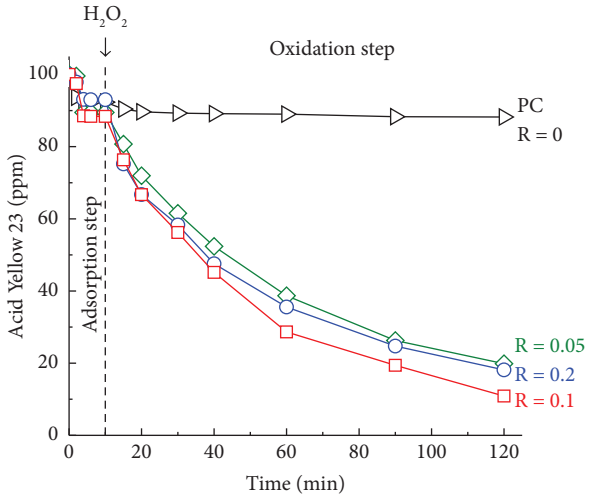

Figure 12: Effect of MPC catalysts prepared from different $FeCl_3$/NF mass ratios on AY23 decolorization (0.80 g/L MPC-Rx-2.0 h, pH 3.0, and 200 ppm H_2O_2).

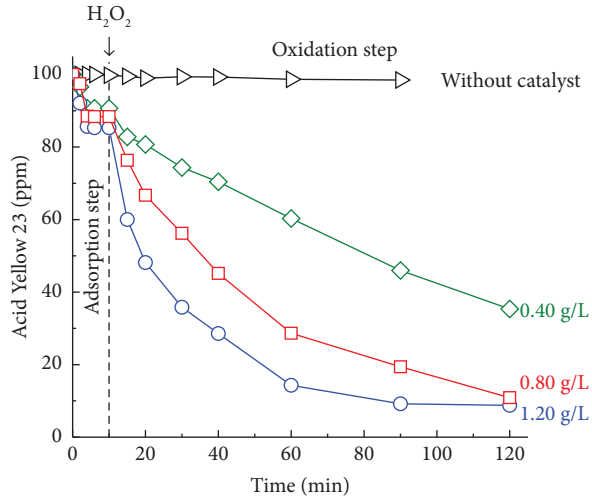

Figure 13: Effect of MPC dosage on AY23 decolorization (MPC-R0.1-2.0 h, pH 3.0, and 200 ppm H_2O_2).

91.2%, respectively. It is advantageous to raise the MPC dosage in order to improve the decolorization efficiency, since this will improve the radical generation. The catalyst cannot, however, be added without limitation [76]. As shown in equation (7), excessive Fe(II) may consume ·OH radicals, resulting in a detrimental effect on AY23 decolorization.

3.2.5. Effect of Initial pH. The effect of the initial pH values on the adsorption capacity and catalytic decolorization of AY23 by MPC is depicted in Figure 14. The pH values ranged from 2.0 to 10.0, while all other variables were kept constant, as shown in Table 3. In general, as pH climbed from 2.0 to 10.0, the adsorption capacity reduced from 18.1 to 6.1 mg/g. According to Vargas et al. [73], the electrostatic interaction between AY23 molecules and carbon surface is favorable at

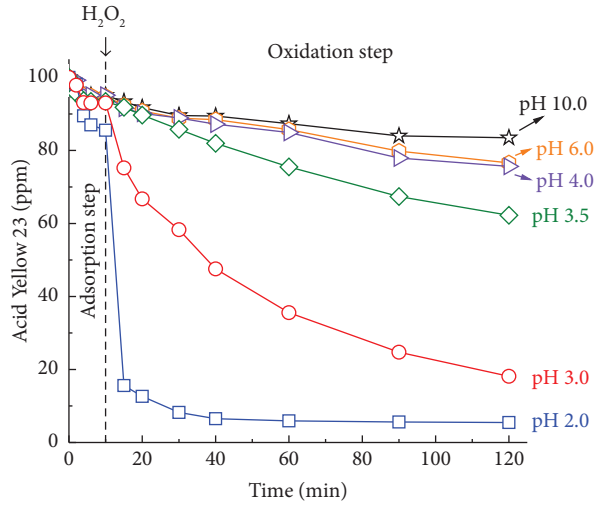

Figure 14: Effect of pH on AY23 decolorization using MPC catalyst (0.80 g/L MPC-R0.1–2.0 h, 200 ppm H_2O_2).

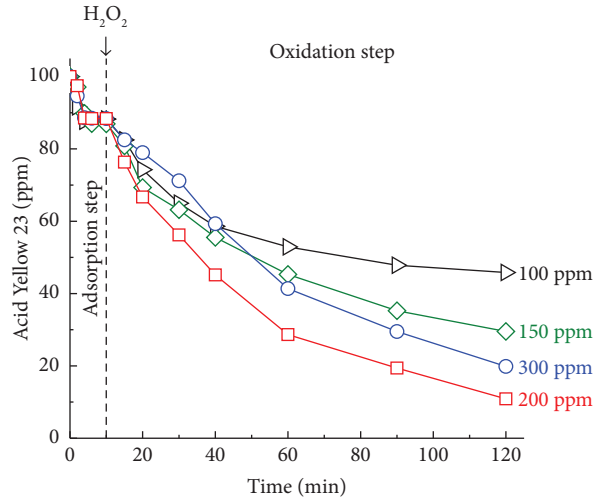

Figure 15: Effect of H_2O_2 dosage on AY23 decolorization using MPC catalyst (0.80 g/L MPC-R0.1–2.0 h, pH 3.0, 200 ppm H_2O_2).

pH ~2. At pH values greater than ~2, sulfonic groups and N=N bonds in AY23 molecules become partially negative, causing electrostatic repulsion with the carbon surface charge.

Initial pH strongly influenced the decolorization efficiency. In general, the AY23 decolorization rate decreased when pH increased. After 120 min of treatment, the decolorization efficiencies at pH 2.0, 3.0, 3.5, 4.0, and 10.0 were 94.5, 89.1, 37.8, 24.4, and 16.5%, respectively. Although pH 2.0 offered rapid and complete AY23 decolorization within 30 min of H_2O_2 addition, low pH could promote Fe leaching, leading to a homogeneous mechanism for catalytic decolorization [77]. As pH increases, the interaction between AY23 molecules and the MPC surface might decrease [73]. Moreover, it is known that as pH increases, the oxidation potential of ·OH radicals lowers [76]. In basic environments (pH 10.0), CO_2 generated during AY23 oxidation might be transformed into CO_3^{2-} and HCO_3^-, which could react with ·OH [78]. Overall, pH 3.0 may be appropriate for achieving a heterogeneous mechanism and maintaining high decolorization efficiency.

3.2.6. Effect of H_2O_2 Dosage. H_2O_2 dosage plays an essential role in Fenton-like oxidation. Therefore, different first H_2O_2 concentrations of 100, 150, 200, and 300 ppm were explored for AY23 decolorization (Figure 15). The results show that increasing the H_2O_2 concentration from 100 to 200 ppm increased AY23 decolorization. Higher H_2O_2 dosage could produce more ·OH radicals [77, 79]. However, as the H_2O_2 concentration rose from 200 to 300 ppm, AY23 decolorization was weakened. The corresponding decolorization efficiency decreased from 89.1 to 80.1% after 120 min of treatment. The high H_2O_2 concentration (300 ppm) might result in increased ·OH scavenging capacity. Recombination of ·OH radicals and the reaction of those radicals with H_2O_2 might occur as follows [80]:

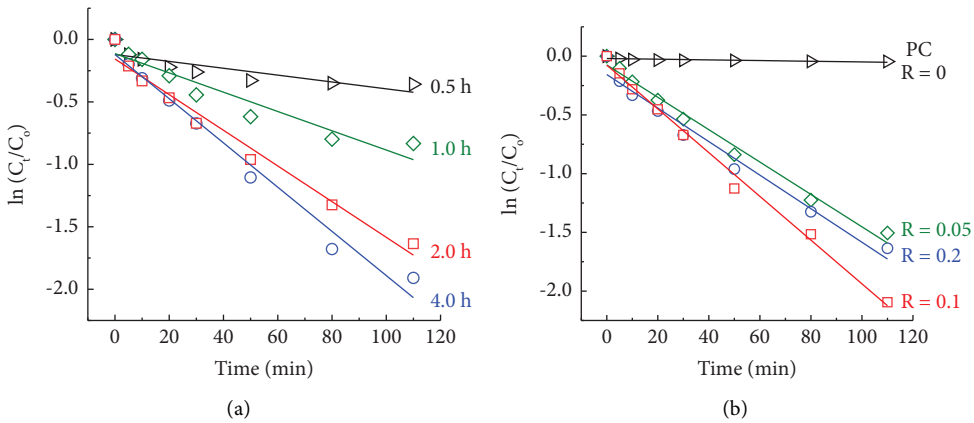

Figure 16: Pseudo-first-order kinetics of AY23 decolorization with MPC catalysts prepared from (a) different pyrolysis time and (b) different $FeCl_3$/NF mass ratios.

$$\begin{aligned} \cdot OH + H_2O_2 &\longrightarrow \cdot OOH + H_2O \\ \cdot OH + \cdot OOH &\longrightarrow O_2 + H_2O \\ \cdot OH + \cdot OH &\longrightarrow H_2O_2 \end{aligned} \quad (8)$$

3.2.7. Kinetics of AY23 Decolorization with MPC Catalysts. The kinetics of AY23 decolorization with different MPC catalysts were examined using a pseudo-first-order model (Figure 16). C_0 and C_t are AY23 concentrations at the beginning and at time t of the oxidation step, respectively. As a consequence, the reaction rate constants (k) for MPC prepared from 0.5-, 1.0-, 2.0-, and 4.0-h pyrolysis were 0.0028 min^{-1} ($R^2 = 0.733$), 0.0077 min^{-1} ($R^2 = 0.914$), 0.0143 min^{-1} ($R^2 = 0.977$), 0.0177 min^{-1} ($R^2 = 0.980$), respectively. Similarly, MPC prepared from $FeCl_3$/NF mass ratios of 0.05, 0.1, and 0.2 had the rate constants of 0.0138 min^{-1} ($R^2 = 0.988$), 0.0186 min^{-1} ($R^2 = 0.993$), and 0.0143 min^{-1} ($R^2 = 0.977$), respectively. These R^2 values from regression lines revealed that the decolorizations generally followed pseudo-first-order kinetics, which is consistent with other earlier investigations using Fe-based catalysts for Fenton-like decolorization of AY23 [10, 77, 80].

4. Conclusion

In this research, magnetic porous carbon was facilely prepared through one-step pyrolysis of $FeCl_3$-impregnated nipa frond. The results showed that Fe_3O_4 and Fe^0 crystals were formed from $FeCl_3$ in carbon support. Notably, these reductions activated the porous structure of carbon, providing a high S_{BET} of 330 m^2/g and a large V_{total} of 0.26 cm^3/g. MPC was accordingly utilized as an oxidation catalyst for acid yellow 23 decolorization by H_2O_2. At pH 3.0, 200 ppm H_2O_2, and 0.80 g/L MPC-R0.1-2 h, AY23 was removed with an adsorption capacity of 14.5 mg/g. Next, 89.1% of AY23 was removed after H_2O_2 addition. Furthermore, AY23 decolorization with MPC catalysts approximated pseudo-first-order kinetics with a typical rate constant of 0.0186 min^{-1}. With a strong saturation magnetization of 7.65 emu/g, MPC catalyst could be easily separated from the reaction mixture using a magnet. In conclusion, environmentally friendly, sustainable, and cheap magnetic porous carbon has the potential to be an efficient catalyst for acid yellow 23 remediation in wastewater.

Abbreviations

NF: Nipa frond
AY23: Acid yellow 23
PC: Porous carbon
MPC: Magnetic porous carbon
XRD: X-ray diffraction
SEM: Scanning electron microscope
EDX: Energy-dispersive X-ray
VSM: Vibrating sample magnetometer
FTIR: Fourier-transform infrared.

Data Availability

No new data were created or analyzed in this study.

Conflicts of Interest

The authors declare that they have no conflicts of interest.

Acknowledgments

We acknowledge Ho Chi Minh City University of Technology (HCMUT), VNU-HCM for supporting this study.

References

[1] S. H. Tabrizi, B. Tanhaei, A. Ayati, and S. Ranjbari, "Substantial improvement in the adsorption behavior of montmorillonite toward tartrazine through hexadecylamine impregnation," *Environmental Research*, vol. 204, Article ID 111965, 2022.

[2] W. You, L. Liu, J. Xu, T. Jin, L. Fu, and Y. Pan, "Effect of anions and cations on tartrazine removal by the zero-valent iron/peroxymonosulfate process: efficiency and major radicals," *Catalysts*, vol. 12, no. 10, p. 1114, 2022.

[3] S. Ranjbari, A. Ayati, B. Tanhaei, A. Al-Othman, and F. Karimi, "The surfactant-ionic liquid bi-functionalization of chitosan beads for their adsorption performance improvement toward tartrazine," *Environmental Research*, vol. 204, Article ID 111961, 2022.

[4] P. Balamurugan, P. S. Kumar, K. Shankar, R. Nagavinothini, and K. Vijayasurya, "Non-carcinogenic risk assessment of groundwater in southern part of Salem district in Tamilnadu, India," *Journal of the Chilean Chemical Society*, vol. 65, no. 1, pp. 4697–4707, 2020.

[5] S. V. Mukate, D. B. Panaskar, V. M. Wagh, and S. J. Baker, "Understanding the influence of industrial and agricultural land uses on groundwater quality in semiarid region of Solapur, India," *Environment, Development and Sustainability*, vol. 22, no. 4, pp. 3207–3238, India, 2020.

[6] M. T. Yagub, T. K. Sen, S. Afroze, and H. M. Ang, "Dye and its removal from aqueous solution by adsorption: a review," *Advances in Colloid and Interface Science*, vol. 209, pp. 172–184, 2014.

[7] E. Gayathiri, P. Prakash, K. Selvam et al., "Plant microbe based remediation approaches in dye removal: a review," *Bioengineered*, vol. 13, no. 3, pp. 7798–7828, 2022.

[8] Y. Cao, G. Yuan, Y. Guo, X. Hu, G. Fang, and S. Wang, "Facile synthesis of TiO_2/g-C_3N_4 nanosheet heterojunctions for efficient photocatalytic degradation of tartrazine under simulated sunlight," *Applied Surface Science*, vol. 600, Article ID 154169, 2022.

[9] S. Zhang, A. Khan, N. Ali et al., "Designing, characterization, and evaluation of chitosan-zinc selenide nanoparticles for visible-light-induced degradation of tartrazine and sunset yellow dyes," *Environmental Research*, vol. 213, Article ID 113722, 2022.

[10] A. Soufi, H. Hajjaoui, R. Elmoubarki, M. Abdennouri, S. Qourzal, and N. Barka, "Heterogeneous Fenton-like degradation of tartrazine using $CuFe_2O_4$ nanoparticles synthesized by sol-gel combustion," *Applied Surface Science Advances*, vol. 9, Article ID 100251, 2022.

[11] G. Stevanović, N. Jović-Jovičić, J. Krstić et al., "Nanocomposite Co-catalysts, based on smectite and biowaste-derived carbon, as peroxymonosulfate activators in degradation of tartrazine," *Applied Clay Science*, vol. 230, Article ID 106718, 2022.

[12] E. Bahadori, V. Vaiano, S. Esposito, M. Armandi, D. Sannino, and B. Bonelli, "Photo-activated degradation of tartrazine by H_2O_2 as catalyzed by both bare and Fe-doped methylimogolite nanotubes," *Catalysis Today*, vol. 304, pp. 199–207, 2018.

[13] N. S. Eroi, A. S. Ello, D. Diabaté, and K. R. Koffi, "Kinetic study of the removal of methyl orange dye by coupling WO_3/H_2O_2," *Journal of Chemistry*, vol. 2022, Article ID 8633545, 8 pages, 2022.

[14] M. Munoz, Z. M. de Pedro, J. A. Casas, and J. J. Rodriguez, "Preparation of magnetite-based catalysts and their application in heterogeneous Fenton oxidation – a review," *Applied Catalysis B: Environmental*, vol. 176-177, pp. 249–265, 2015.

[15] S. Zeng and E. Kan, "$FeCl_3$-activated biochar catalyst for heterogeneous Fenton oxidation of antibiotic sulfamethoxazole in water," *Chemosphere*, vol. 306, Article ID 135554, 2022.

[16] J. Wang and J. Tang, "Fe-based Fenton-like catalysts for water treatment: preparation, characterization and modification," *Chemosphere*, vol. 276, Article ID 130177, 2021.

[17] N. Thomas, D. D. Dionysiou, and S. C. Pillai, "Heterogeneous Fenton catalysts: a review of recent advances," *Journal of Hazardous Materials*, vol. 404, Article ID 124082, 2021.

[18] C. S. D. Rodrigues, O. S. G. P. Soares, M. T. Pinho, M. F. R. Pereira, and L. M. Madeira, "p-Nitrophenol degradation by heterogeneous Fenton's oxidation over activated carbon-based catalysts," *Applied Catalysis B: Environmental*, vol. 219, pp. 109–122, 2017.

[19] M. D. Nguyen, H. V. Tran, S. Xu, and T. R. Lee, "Fe_3O_4 nanoparticles: structures, synthesis, magnetic properties, surface functionalization, and emerging applications," *Applied Sciences*, vol. 11, no. 23, Article ID 11301, 2021.

[20] D. V. Nguyen, H. N. Do, H. N. Do, and L. Q. Nguyen, "One-step preparation of rice husk-based magnetic biochar and its catalytic activity for p-nitrophenol degradation," *Chemical Engineering Transactions*, vol. 78, pp. 379–384, 2020.

[21] Z. Chen, Y. Ma, B. Geng, M. Wang, and X. Sun, "Photocatalytic performance and magnetic separation of TiO_2-functionalized γ-Fe_2O_3, Fe, and Fe/Fe_2O_3 magnetic particles," *Journal of Alloys and Compounds*, vol. 700, pp. 113–121, 2017.

[22] Z. Feng, R. Yuan, F. Wang, Z. Chen, B. Zhou, and H. Chen, "Preparation of magnetic biochar and its application in catalytic degradation of organic pollutants: a review," *The Science of the Total Environment*, vol. 765, Article ID 142673, 2021.

[23] L. Xin, J. Hu, Y. Xiang et al., "Carbon-based nanocomposites as Fenton-like catalysts in wastewater treatment applications: a review," *Materials*, vol. 14, no. 10, p. 2643, 2021.

[24] Z. I. Pan and X. F. Qian, "Porous carbons for use in electro-Fenton and Fenton-like reactions," *Carbon*, vol. 192, no. 1, pp. 484-485, 2022.

[25] J. Wang and S. Wang, "Preparation, modification and environmental application of biochar: a review," *Journal of Cleaner Production*, vol. 227, pp. 1002–1022, 2019.

[26] S. Chhabria, A. V. Raghavendra Rao, V. Naga Lakshmi et al., "Valorization of hazardous materials along with biomass for green energy generation and environmental sustainability through pyrolysis," *Journal of Chemistry*, vol. 2022, Article ID 2215883, 9 pages, 2022.

[27] X. Tan, Y. Liu, G. Zeng et al., "Application of biochar for the removal of pollutants from aqueous solutions," *Chemosphere*, vol. 125, pp. 70–85, 2015.

[28] A. G. Kumi, M. G. Ibrahim, M. Nasr, and M. Fujii, "Biochar synthesis for industrial wastewater treatment: a critical review," *Materials Science Forum*, vol. 1008, pp. 202–212, 2020.

[29] W. Xiang, X. Zhang, J. Chen et al., "Biochar technology in wastewater treatment: a critical review," *Chemosphere*, vol. 252, Article ID 126539, 2020.

[30] J. Qu, J. Shi, Y. Wang et al., "Applications of functionalized magnetic biochar in environmental remediation: a review," *Journal of Hazardous Materials*, vol. 434, Article ID 128841, 2022.

[31] K. R. Thines, E. C. Abdullah, N. M. Mubarak, and M. Ruthiraan, "Synthesis of magnetic biochar from agricultural waste biomass to enhancing route for waste water and polymer application: a review," *Renewable and Sustainable Energy Reviews*, vol. 67, pp. 257–276, 2017.

[32] M. T. H. Siddiqui, S. Nizamuddin, H. A. Baloch et al., "Fabrication of advance magnetic carbon nano-materials and their potential applications: a review," *Journal of Environmental Chemical Engineering*, vol. 7, no. 1, Article ID 102812, 2019.

[33] W. Astuti, T. Sulistyaningsih, D. Prastiyanto, B. S. A. Purba, and R. Kusumawardani, "Synthesis of magnetically separable

activated carbon from pineapple crown leaf for zinc ion removal," *Materials Science Forum*, vol. 1007, pp. 71–75, 2020.

[34] Z. Wu, W. Li, P. A. Webley, and D. Zhao, "General and controllable synthesis of novel mesoporous magnetic iron oxide@carbon encapsulates for efficient arsenic removal," *Advanced Materials*, vol. 24, no. 4, pp. 485–491, 2012.

[35] J. Bedia, M. Peñas-Garzón, A. Gómez-Avilés, J. J. Rodriguez, and C. Belver, "Review on activated carbons by chemical activation with $FeCl_3$," *C*, vol. 6, no. 2, p. 21, 2020.

[36] T. V. T. Do, Q. L. N. Bui, H. M. Nguyen et al., "One-pot fabrication of magnetic biochar by $FeCl_3$-activation of lotus seedpod and its catalytic activity towards degradation of Orange G," *Materials Research Express*, vol. 9, no. 10, Article ID 105601, 2022, https://iopscience.iop.org/article/10.1088/2053-1591/ac9819/meta.

[37] A. N. T. Le, H. H. Lam, T. M. Tran-Thuy et al., "Facile preparation of multifunctional Ag-Fe_xO_y/C composite from coffee husk for antibacterial and catalytic applications," *Advances in Science and Technology*, vol. 122, pp. 3–9, 2023.

[38] H. M. Nguyen, H. N. Do, H. N. Do et al., "Direct synthesis of magnetic porous carbon from coconut husk and its application in catalytic degradation of p-nitrophenol by H_2O_2," *VNUHCM Journal of Engineering and Technology*, vol. 5, no. SI1, pp. 120–127, 2023.

[39] P. Liu, H. Li, X. Liu, Y. Wan, X. Han, and W. Zou, "Preparation of magnetic biochar obtained from one-step pyrolysis of salix mongolica and investigation into adsorption behavior of sulfadimidine sodium and norfloxacin in aqueous solution," *Journal of Dispersion Science and Technology*, vol. 41, no. 2, pp. 214–226, 2020.

[40] J. Fan, X. Xu, Q. Ni et al., "Enhanced as (V) removal from aqueous solution by biochar prepared from iron-impregnated corn straw," *Journal of Chemistry*, vol. 2018, Article ID 5137694, pp. 1–8, 2018.

[41] J. Bedia, V. M. Monsalvo, J. J. Rodriguez, and A. F. Mohedano, "Iron catalysts by chemical activation of sewage sludge with $FeCl_3$ for CWPO," *Chemical Engineering Journal*, vol. 318, pp. 224–230, 2017.

[42] H. Lyu, Q. Zhang, and B. Shen, "Application of biochar and its composites in catalysis," *Chemosphere*, vol. 240, Article ID 124842, 2020.

[43] L. S. Hamilton and D. H. Murphy, "Use and management of nipa palm (*Nypa fruticans*, arecaceae): a review," *Economic Botany*, vol. 42, no. 2, pp. 206–213, 1988.

[44] D. V. Nguyen, H. Rabemanolontsoa, and S. Saka, "Fed-batch fermentation of nipa sap to acetic acid by *Moorella thermoacetica* (f. *Clostridium thermoaceticum*)," *Chemical Industry and Chemical Engineering Quarterly*, vol. 23, no. 4, pp. 507–514, 2017.

[45] D. V. Nguyen, H. Rabemanolontsoa, and S. Saka, "Sap from various palms as a renewable energy source for bioethanol production," *Chemical Industry and Chemical Engineering Quarterly*, vol. 22, no. 4, pp. 355–373, 2016.

[46] P. Tamunaidu, N. Matsui, Y. Okimori, and S. Saka, "Nipa (*Nypa fruticans*) sap as a potential feedstock for ethanol production," *Biomass and Bioenergy*, vol. 52, pp. 96–102, 2013.

[47] P. Tamunaidu and S. Saka, "Comparative study of nutrient supplements and natural inorganic components in ethanolic fermentation of nipa sap," *Journal of the Japan Institute of Energy*, vol. 92, no. 2, pp. 181–186, 2013.

[48] P. Tamunaidu and S. Saka, "Chemical characterization of various parts of nipa palm (*Nypa fruticans*)," *Industrial Crops and Products*, vol. 34, no. 3, pp. 1423–1428, 2011.

[49] N. Phaiboonsilpa, P. Tamunaidu, and S. Saka, "Two-step hydrolysis of nipa (*Nypa fruticans*) frond as treated by semi-flow hot-compressed water," *Holzforschung*, vol. 65, no. 5, pp. 659–666, 2011.

[50] S. Evelyn, D. Andrio, D. Andrio, A. Aman, and H. Ohi, "*Nypa fruticans* frond waste for pure cellulose utilizing sulphur-free and totally chlorine-free processes," *Molecules*, vol. 27, no. 17, p. 5662, 2022.

[51] E. Viollier, P. W. Inglett, K. Hunter, A. N. Roychoudhury, and P. Van Cappellen, "The ferrozine method revisited: Fe(II)/Fe(III) determination in natural waters," *Applied Geochemistry*, vol. 15, no. 6, pp. 785–790, 2000.

[52] S. Zhang, Y. Su, S. Zhu, H. Zhang, and Q. Zhang, "Effects of pretreatment and $FeCl_3$ preload of rice husk on synthesis of magnetic carbon composites by pyrolysis for supercapacitor application," *Journal of Analytical and Applied Pyrolysis*, vol. 135, pp. 22–31, 2018.

[53] E. M. Abdelrazek, "Influence of $FeCl_3$ filler on the structure and physical properties of polyethyl-methacrylate films," *Physica B: Condensed Matter*, vol. 400, no. 1-2, pp. 26–32, 2007.

[54] E. Uzun, "Production of ferric complex compounds for wastewater treatment from hot rolled iron-steel solid waste," *International Journal of Materials Engineering and Technology*, vol. 2, no. 1, pp. 1–7, 2019.

[55] S. Zhou, K. You, H. Gao et al., "Mesoporous silica-immobilized $FeCl_3$ as a highly efficient and recyclable catalyst for the nitration of benzene with NO_2 to nitrobenzene," *Molecular Catalysis*, vol. 433, pp. 91–99, 2017.

[56] S. M. Nasef, N. Badawy, F. Hafez, S. Slim, and E. M. El Nesr, "Preparation and characterization of magnetic nanocomposite based on gum Arabic/2-hydroxyethylmethacrylate using gamma irradiation for use in biomedical application," *Arab Journal of Nuclear Sciences and Applications*, vol. 52, no. 2, pp. 209–226, 2019.

[57] H. M. Nguyen, L. T. Nguyen, L. T. K. Nguyen et al., "Facile preparation of lotus seedpod-derived magnetic porous carbon for catalytic oxidation of Ponceau 4R," *IOP Conference Series: Earth and Environmental Science*, vol. 947, no. 1, Article ID 012019, 2021.

[58] T. Horikawa, D. D. Do, and D. Nicholson, "Capillary condensation of adsorbates in porous materials," *Advances in Colloid and Interface Science*, vol. 169, no. 1, pp. 40–58, 2011.

[59] M. Ahmad, A. U. Rajapaksha, J. E. Lim et al., "Biochar as a sorbent for contaminant management in soil and water: a review," *Chemosphere*, vol. 99, pp. 19–33, 2014.

[60] W. J. Liu, K. Tian, H. Jiang, and H. Q. Yu, "Facile synthesis of highly efficient and recyclable magnetic solid acid from biomass waste," *Scientific Reports*, vol. 3, no. 1, p. 2419, 2013.

[61] S. Chen, X. Li, J. Wu et al., "*Plumula Nelumbinis*: a review of traditional uses, phytochemistry, pharmacology, pharmacokinetics and safety," *Journal of Ethnopharmacology*, vol. 266, Article ID 113429, 2021.

[62] K. L. Chiu and D. H. L. Ng, "Synthesis and characterization of cotton-made activated carbon fiber and its adsorption of methylene blue in water treatment," *Biomass and Bioenergy*, vol. 46, pp. 102–110, 2012.

[63] X. Liu, J. Liao, H. Song, Y. Yang, C. Guan, and Z. Zhang, "A biochar-based route for environmentally friendly controlled release of nitrogen: urea-loaded biochar and bentonite composite," *Scientific Reports*, vol. 9, no. 1, p. 9548, 2019.

[64] H. Zhang, G. Xue, H. Chen, and X. Li, "Magnetic biochar catalyst derived from biological sludge and ferric sludge using hydrothermal carbonization: preparation, characterization

and its circulation in Fenton process for dyeing wastewater treatment," *Chemosphere*, vol. 191, pp. 64–71, 2018.

[65] Y. Liu, S. P. Sohi, S. Liu, J. Guan, J. Zhou, and J. Chen, "Adsorption and reductive degradation of Cr(VI) and TCE by a simply synthesized zero valent iron magnetic biochar," *Journal of Environmental Management*, vol. 235, pp. 276–281, 2019.

[66] P. Huang, Z. Ye, W. Xie et al., "Rapid magnetic removal of aqueous heavy metals and their relevant mechanisms using nanoscale zero valent iron (nZVI) particles," *Water Research*, vol. 47, no. 12, pp. 4050–4058, 2013.

[67] B. S. Yadav, R. Singh, A. K. Vishwakarma, and N. Kumar, "Facile synthesis of substantially magnetic hollow nanospheres of maghemite (γ-Fe_2O_3) originated from magnetite (Fe_3O_4) via solvothermal method," *Journal of Superconductivity and Novel Magnetism*, vol. 33, no. 7, pp. 2199–2208, 2020.

[68] Y. Wei, B. Han, X. Hu, Y. Lin, X. Wang, and X. Deng, "Synthesis of Fe_3O_4 nanoparticles and their magnetic properties," *Procedia Engineering*, vol. 27, pp. 632–637, 2012.

[69] J. Sun, S. Zhou, P. Hou et al., "Synthesis and characterization of biocompatible Fe_3O_4 nanoparticles," *Journal of Biomedical Materials Research Part A*, vol. 80, no. 2, pp. 333–341, 2007.

[70] E. M. Abd El-Monaem, A. M. Omer, G. M. El-Subruiti, M. S. Mohy-Eldin, and A. S. Eltaweil, "Zero-valent iron supported-lemon derived biochar for ultra-fast adsorption of methylene blue," *Biomass Conversion and Biorefinery*, 2022.

[71] M. J. Bonder, Y. Zhang, K. L. Kiick, V. Papaefthymiou, and G. C. Hadjipanayis, "Controlling synthesis of Fe nanoparticles with polyethylene glycol," *Journal of Magnetism and Magnetic Materials*, vol. 311, no. 2, pp. 658–664, 2007.

[72] N. A. D. Burke, H. D. H. Stover, F. P. Dawson, J. D. Lavers, P. K. Jain, and H. Oka, "Preparation and characterization of polymer-coated magnetic nanoparticles," *IEEE Transactions on Magnetics*, vol. 37, no. 4, pp. 2660–2662, 2001.

[73] A. M. M. Vargas, A. L. Cazetta, A. C. Martins et al., "Kinetic and equilibrium studies: adsorption of food dyes Acid Yellow 6, Acid Yellow 23, and Acid Red 18 on activated carbon from flamboyant pods," *Chemical Engineering Journal*, vol. 181-182, pp. 243–250, 2012.

[74] J. Rodriguez, J. M. Ochando-Pulido, and A. Martinez-Ferez, "The effect of pH in tannery wastewater by Fenton vs. heterogeneous Fenton process," *Chemical Engineering Transactions*, vol. 73, pp. 205–210, 2019.

[75] H. El Ghandoor, H. Zidan, M. M. Khalil, and M. Ismail, "Synthesis and some physical properties of magnetite (Fe_3O_4) nanoparticles," *International Journal of Electrochemical Science*, vol. 7, no. 6, pp. 5734–5745, 2012.

[76] N. Wang, T. Zheng, G. Zhang, and P. Wang, "A review on Fenton-like processes for organic wastewater treatment," *Journal of Environmental Chemical Engineering*, vol. 4, no. 1, pp. 762–787, 2016.

[77] T. G. Merlain, L. T. Nanganoa, B. B. P. Desire, N. J. Nsami, and K. J. Mbadcam, "Fenton-like oxidation of Acid Yellow 23 in the presence of iron rich soil," *Advances in Chemical Engineering and Science*, vol. 6, no. 5, pp. 553–569, 2016.

[78] S. M. Kumar, "Degradation and mineralization, of organic contaminants by Fenton and photo-Fenton processes: review of mechanisms and effects of organic and inorganic additives," *Research Journal of Chemistry and Environment*, vol. 15, no. 2, pp. 96–112, 2011.

[79] N. Modirshahla, M. A. Behnajady, and F. Ghanbary, "Decolorization and mineralization of C.I. Acid Yellow 23 by Fenton and photo-Fenton processes," *Dyes and Pigments*, vol. 73, no. 3, pp. 305–310, 2007.

[80] A. V. Russo, B. G. Merlo, and S. E. Jacobo, "Adsorption and catalytic degradation of tartrazine in aqueous medium by a Fe-modified zeolite," *Cleaner Engineering and Technology*, vol. 4, Article ID 100211, 2021.